Relativistic force between fast electrons and planar targets

2014 New J. Phys. 16 073048

(http://iopscience.iop.org/1367-2630/16/7/073048)

New Journal of Physics
The open access journal at the forefront of physics
Deutsche Physikalische Gesellschaft DPG | IOP Institute of Physics

Relativistic force between fast electrons and planar targets

A Rivacoba[1,2] **and N Zabala**[1,3]

[1] Materials Physics Center CSIC-UPV/EHU and Donostia International Physics Center DIPC, Paseo Manuel Lardizabal 4, 20018 Donostia-San Sebastian, Spain
[2] Department of Materials Physics, Faculty of Chemistry, UPV/EHU, 20080 Donostia, Spain
[3] Department of Electricity and Electronics, Faculty of Science and Technology, UPV/EHU, 48080 Bilbao, Spain
E-mail: alberto.rivacoba@ehu.es

Received 27 March 2014, revised 29 May 2014
Accepted for publication 19 June 2014
Published 30 July 2014

New Journal of Physics **16** (2014) 073048

doi:10.1088/1367-2630/16/7/073048

Abstract

The full retarded electromagnetic force experienced by swift electrons moving parallel to planar boundaries is revisited, for both metallic and dielectric targets, with special emphasis on the consequences in electron microscopy experiments. The focus is placed on the sign of the transverse force experienced by the electron beam as a function of the impact parameter. For point probes, the force is found to be always attractive. The contribution of the induced magnetic field and the causality requirements of the target dielectric response, given by the Kramers–Kronig (K–K) relations, prove to be crucial issues at small impact parameters. For spatially extended probes, repulsive forces are predicted for close trajectories, in agreement with previous works. The force experienced by the target is also explored, with the finding that in insulators, the momentum associated to Cherenkov radiation (CR) is relevant at large impact parameters.

Keywords: electromagnetic force, electron beams, surface plasmon, dielectric function, cherenkov radiation

1. Introduction

Although the force between moving electrons and bounded media is a well studied problem, recent experiments and new calculations have questioned its sign. Besides the apparent simplicity of the system, when the spatial extension of the beam is considered, or the complexity in the electromagnetic response of the medium is accounted for, counter-intuitive effects may arise [1–3].

The retarding force along an electron's trajectory in an inhomogeneous medium has attracted the most attention in recent decades due to its interest for electron energy loss spectroscopy (EELS) in scanning transmission electron microscopy (STEM) [4, 5]. Nowadays this technique has become a very accurate tool currently used to characterize nanostructures and map plasmons in space with high resolution [6, 7].

The transverse component of the force has received less attention, but in general it is assumed to be attractive and small, so that the electron trajectory is unaffected by the interaction with the target. Nevertheless, several experiments have questioned the expected behavior. For instance, three decades ago Cowley [8, 9] reported strong deflections of about 10^{-3} rad (attractive) when a 100 keV electron beam passed close to targets of magnesium oxide (MgO) and gold (Au) of 100 nm side at a distance of around 1 nm. These experiments stimulated different calculations of the image force within non-retarded classical dielectric theory [10–12], considering infinite planar surfaces or spherical targets [13]. Although these approaches satisfactorily explained the energy losses, they predicted deflections three orders of magnitude smaller that the observed ones. García–Molina *et al* [14] calculated both components of the force including retardation effects, but they did not include the magnetic field contribution to the transverse component of the force on the ground that for moderately relativistic probes (80 keV), it was negligible. Forstmann *et al* [15] studied the energy loss of electrons interacting with non-abrupt surfaces as a problem of optics, i.e., by calculating the reflection at the surface of the electromagnetic fields of the external beam. In the context of particle accelerators, Schieber and Schächter [16] studied the reaction forces on relativistic particles moving above a dielectric or metallic interface by distinguishing the contribution of evanescent and propagating waves, in the cases when Cherenkov radiation (CR) is emitted. They found that the evanescent contribution is always attractive, whereas the Cherenkov part reverses its sign for very high velocities. However, the total transverse force remains always attractive.

More recently, this problem has received a further boost by the possibility of manipulating metallic nanoparticles (NPs) with electron beams, in a similar way to optical tweezers, by transferring linear and angular momenta [4, 17] to the target. Recent advances in electron microscopy allow monitoring of the movement of nanometric gold particles under the action of a well-focused electron beam, finding that the force experienced by the particle becomes repulsive at small impact parameters [18, 19]. These experiments have stimulated new relativistic calculations accounting for a precise description of the target [3, 20] which reproduce the observed repulsive interaction; however, the physics behind this effect is still unclear. The electromagnetic interaction is not the only mechanism able to explain this anomalous momentum transfer. Batson *et al* [3] have pointed out the possibility of other mechanisms leading to the repulsive behavior: namely, the secondary electron emission and electron diffraction.

In most of these theoretical approaches the probe, assumed to be a point charge, is described as a classical particle. Several works have concluded that, for fast probes, the non-

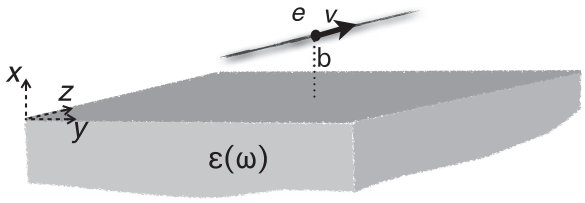

Figure 1. Point charge moving in vacuum with velocity **v** parallel to a planar boundary with a medium of permittivity $\epsilon(\omega)$, at impact parameter b.

retarded quantal effects in EELS may be understood in terms of the classical result averaged out over the lateral extension of the beam [21, 22]. Furthermore, the beam spatial extension is an interesting issue in the case of coherent extended probes. In fact, recent experiments performed with spatially extended coherent electron probes at low energies (1.6 keV) have shown a loss of coherence as an effect of the scattering with a large flat surface [23]. These results have been explained in terms of the inelastic interaction of the electron with the target [24]. In the ultrarelativistic limit, at energies and beam widths well above those of the actual STEM setups, Rebernik [1] demonstrated that the interaction between a surface and a charge packet moving paralell to it can become repulsive above a critical relativistic energy. Later, Rebernik and Podgornik [2] have predicted that the interaction becomes repulsive even for point charges when the medium is an uniaxial dielectric.

The aim of this study is to shed light on the different factors which determine the sign of the force in the simplest geometry. We calculate the electromagnetic force experienced by relativistic electrons of energies commonly used in EELS experiments (in the range 100–400 keV), placing the focus on the transverse component and analyzing the role played by the electric and magnetic components of the Lorentz force as the impact parameter and the velocity of the beam are varied. We consider typical metals as aluminum (Al), described with the Drude function, or Au, characterized both with a parametrized Drude–Lorentz function and experimental data. Experimental data are also used in the study of a MgO interface, an insulator presenting a band gap below 6.8 eV, so that it provides an energy window open for emission of CR. In the cases where experimental dielectric data are used, we discuss the need for causal response functions, verifying the Kramers–Kronig (K–K) constraints. This is a consequence of the very large range of frequencies contributing significantly to the transverse force for beam trajectories close to the surface. Finally, we compare the force exerted by the electron on the dielectric medium, calculated through the Maxwell stress tensor, with that experienced by the probe.

In the derivation of analytical expressions, atomic (a.u.) and electromagnetic Gaussian units are used.

2. Force on a point electron probe moving parallel to a planar interface

We consider first the force experienced by a point electron moving in vacuum with velocity **v**, parallel to a planar boundary ($x = 0$) of a medium characterized by a local dielectric function $\epsilon(\omega)$, as depicted in figure 1. The corresponding current density is $\mathbf{J} = \mathbf{v}\delta(x - b)\delta(y)\delta(z - vt)$, and the resulting force on the electron is the Lorentz force $\mathbf{F} = \mathbf{E} + c^{-1}\mathbf{v} \times \mathbf{B}$, where **E** and **B** are the induced electric and magnetic fields evaluated at the charge position. The induced

electromagnetic field is obtained as the solution [14] of the wave equation for the potentials in subspaces $x < 0$ and $x > 0$, using the boundary conditions at the interface $x = 0$. The solutions derived for the three spatial components of the fields in both subspaces are given in appendix A. From them, it is straightforward to obtain the expressions for the transverse (F_x) and longitudinal (F_z) components of the force, which are written in terms of a single response function Σ of both frequency ω and the parallel component of the momentum k_y:

$$F_x = \frac{-2}{\pi v}\int_0^\infty dk_y \int_0^\infty d\omega \nu_0 \,\mathrm{Re}\left[\Sigma\left(k_y,\,\omega\right)\right]e^{-2\nu_0 b} \tag{1}$$

$$F_z = \frac{-2}{\pi v}\int_0^\infty dk_y \int_0^\infty d\omega \frac{\omega}{v}\,\mathrm{Im}\left[\Sigma\left(k_y,\,\omega\right)\right]e^{-2\nu_0 b}, \tag{2}$$

where

$$\Sigma\left(k_y,\,\omega\right) = \frac{1}{(\nu+\nu_0)\nu_0}\left[\frac{2\nu_0^2(\epsilon-1)}{\nu+\nu_0\epsilon} + \gamma^{-2}(\nu-\nu_0)\right], \tag{3}$$

$\nu = \sqrt{k_y^2 + [1-\beta^2\epsilon(\omega)]\omega^2/v^2}$, $\nu_0 = \sqrt{k_y^2 + \omega^2/\gamma^2 v^2}$, $\beta = v/c$, and $\gamma = (1-\beta^2)^{-1/2}$ is the Lorentz factor.

These expressions are equivalent to the ones reported in [16]. Notice that, although the longitudinal component (the stopping power) agrees with the expression given by García Molina *et al* [14], the transverse one is not the same, because the authors neglect the magnetic contribution to the Lorentz force. In the limit $\beta \to 0$ the well-known non-relativistic expressions [10, 12] are recovered from equations (1) and (2):

$$F_x = \frac{-2}{\pi v^2}\int_0^\infty d\omega\omega K_1\left(\frac{2\omega b}{v}\right)\mathrm{Re}\left[\frac{\epsilon(\omega)-1}{\epsilon(\omega)+1}\right] \tag{4}$$

$$F_z = \frac{-2}{\pi v^2}\int_0^\infty d\omega\omega K_0\left(\frac{2\omega b}{v}\right)\mathrm{Im}\left[\frac{\epsilon(\omega)-1}{\epsilon(\omega)+1}\right]. \tag{5}$$

Note that $\Sigma(k_y,\,\omega)$ only depends on the parameters of the target and on the velocity of the probe, while the impact parameter dependence lies just on the exponential factor $e^{-2\nu_0 b}$ present in both equations (1) and (2). This function is the characteristic response function of the interface, equivalent to the non-retarded function $(\epsilon-1)/(\epsilon+1)$ in equations (4) and (5), but due to retardation it includes a velocity dependence accounting for the dispersion of surface excitations.

In order to interpret the interaction in terms of scattering events which involve exchange of energy ω and moment transfer $\mathbf{k}$, it is helpful to recast the longitudinal component F_z as:

$$F_z = -\int_0^\infty \omega d\omega \frac{dP}{dz d\omega}, \tag{6}$$

so that the magnitude $dP/dzd\omega$ is interpreted as the probability (per unit length) of losing energy ω:

$$\frac{dP}{dzd\omega} = \frac{2}{\pi v^2}\int_0^\infty dk_y e^{-2\nu_0 b}\,\mathrm{Im}\left[\Sigma\left(k_y,\,\omega\right)\right]. \tag{7}$$

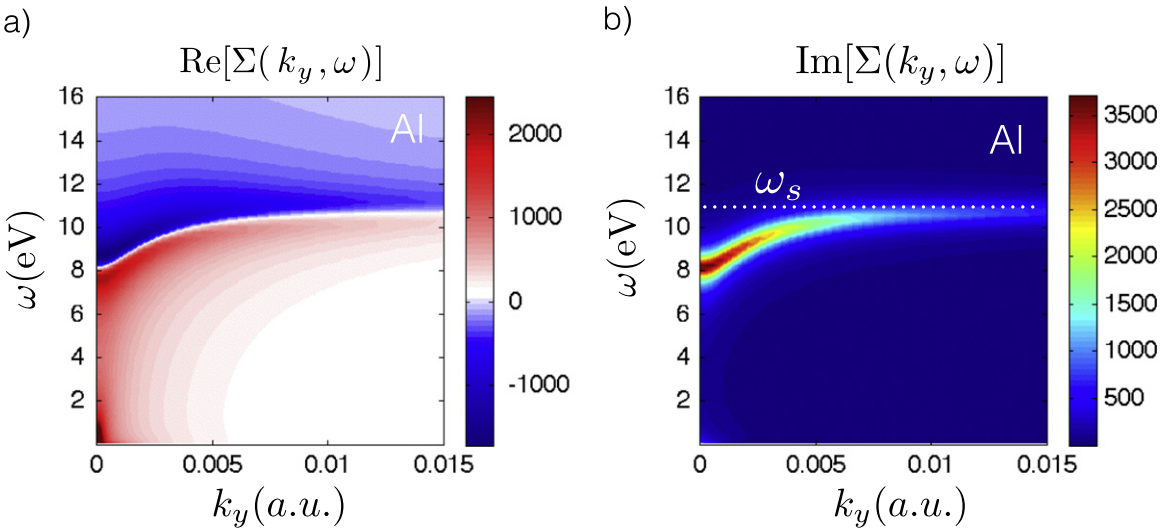

Figure 2. Color maps of (a) real and (b) imaginary parts of $\Sigma(k_y, \omega)$ function vs energy and parallel component of momentum k_y, for a Drude dielectric function corresponding to Al ($\omega_p = 15.3\,\mathrm{eV}$ and $\Gamma = 1\,\mathrm{eV}$). The energy of the probe is 300 keV ($\beta = 0.78$).

The parameter ν_0 may be interpreted as the modulus of k_x, the transverse wave vector component associated to the evanescent fields $k_x = i\nu_0 = \sqrt{\omega^2 c^{-2} - k_y^2 - \omega^2 v^{-2}}$. Then, the momentum transfer per unit length $\Delta\mathbf{p}/\Delta z$ is written as:

$$\frac{\Delta p_x}{\Delta z} = \frac{F_x}{v} = \frac{-2}{\pi v^2}\int_0^\infty dk_y \int_0^\infty d\omega\ \mathrm{Im}\left[k_x \Sigma\left(k_y, \omega\right)\right] e^{-2\nu_0 b}, \tag{8}$$

$$\frac{\Delta p_z}{\Delta z} = \frac{F_z}{v} = \frac{-2}{\pi v^2}\int_0^\infty dk_y \int_0^\infty d\omega k_z\ \mathrm{Im}\left[\Sigma\left(k_y, \omega\right)\right] e^{-2\nu_0 b}, \tag{9}$$

where $k_z = \omega v^{-1}$ is the longitudinal component of the momentum. In this way, the set of equations (7)–(9) provides a description of the scattering of the probe in terms of the creation of excitations of momentum $\mathbf{k} = (k_x, k_y, \omega v^{-1})$ and energy ω. The function Σ describes the probability (always per unit length) of exciting such a process.

In order to visualize the surface excitation spectrum of a metallic interface, we have represented in figure 2 the real and imaginary parts of $\Sigma(k_y, \omega)$ for a Drude function corresponding to aluminum, $\epsilon(\omega) = 1 - \omega_p^2/(\omega(\omega + i\Gamma)$, with $\omega_p = 15.3\,\mathrm{eV}$ and $\Gamma = 1\,\mathrm{eV}$. The energy of the probe is 300 keV ($\beta = 0.78$) in this case, a value which is nowadays available in STEM experiments. The behavior of both the real and imaginary parts of the response function is determined by the surface plasmon dispersion $\omega(k_y)$, which is red shifted with respect to the non-retarded value of the surface plasmon $\omega_s = \omega_p/\sqrt{2}$, recovered for large values of k_y (see [5]). The surface plasmon energy corresponds to the poles of the response function $\Sigma(k_y, \omega)$, i.e. the solution of equation $\nu + \epsilon\nu_0 = 0$, which in its turn leads to the same solution of the dispersion relation $c^2k^2 = \omega^2\epsilon/(\epsilon + 1)$ for excitations with well-defined longitudinal wave vector $k_z = \omega/v$. In figure 3 we show the surface plasmon dispersion $\omega(k_y)$ for different energies of the probe. As expected, the deviation from the flat non-retarded value ω_s is more relevant as the energy of the probe increases and also at large wavelengths of the induced excitations.

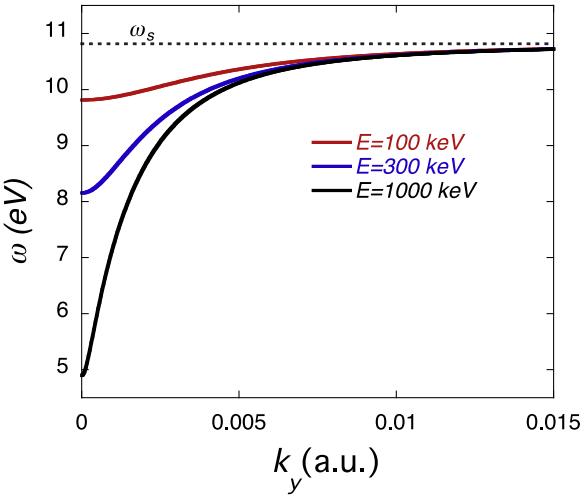

Figure 3. Surface plasmon dispersion curves for a planar semi-infinite medium described by a Drude dielectric function and four different values of the electron probe energy E.

The imaginary part of Σ is always positive and strongly peaked around the surface plasmon dispersion curve. Notice that the exponential factor $e^{-2\nu_0 b}$ involved in the force (equations (1) and (2)), determines the region ($\nu_0 b < 1$) of the k_y-ω plane, significantly contributing to the integrals for a given impact parameter. As a consequence of the dispersion relation, the retardation effects become relevant in the energy loss spectrum ($dP/dzd\omega$) at large impact parameters, where the main contribution arises from small k_y. In the plot of the real part of $\Sigma(k_y, \omega)$ (figure 2(a)), the surface plasmon dispersion curve defines the borderline between positive and negative contributions to the transverse component of the force, showing that the surface plasmon excitations do not contribute to the transverse force.

The retardation effects in transition metals and insulators are more difficult to analyze due to the complexity of their excitation spectrum. An accurate description of the dielectric function of these materials requires the use of experimental data. The case of insulators which are transparent at low frequencies presents an additional interest, because these media can sustain propagating electromagnetic fields given by the term $e^{-\nu x}$ (see appendix A). This is the so-called CR, emerging in the region of the excitation space where ϵ is real and ν purely imaginary, i.e., $k_y^2 < (\omega/v)^2(\epsilon\beta^2 - 1)$. This implies small values of k_y and large values of both the velocity and the real part of the dielectric function in the gap (so that $\epsilon\beta^2 > 1$).

For an insulator of this type, as MgO, the real and imaginary parts of $\Sigma(k_y, \omega)$ are represented in figure 4 for 300 keV electrons. As in the previous example of a Drude metal, we observe that the imaginary part, figure 4(b), is always positive, and the real one, figure 4(a), presents two regions of opposite sign. The color maps of both plots have been truncated in order to enhance the contrast between the different regions, but the contribution in the region where the Cherenkov condition is fulfilled is considerably higher. The energy region ($\omega \leqslant 6.6$ eV) where CR is produced is evident in figure 4(b), where the boundary in the $k_y - \omega$ space for this phenomenon has been traced in a dashed white line.

Although the present work is not focused on the energy loss spectra, for the following analysis it is instructive to discuss first how the features of the function $\Sigma(k_y, \omega)$, as shown in figures 2 and 4, are reflected in the EEL spectra of figure 5, where the retarded and non-retarded

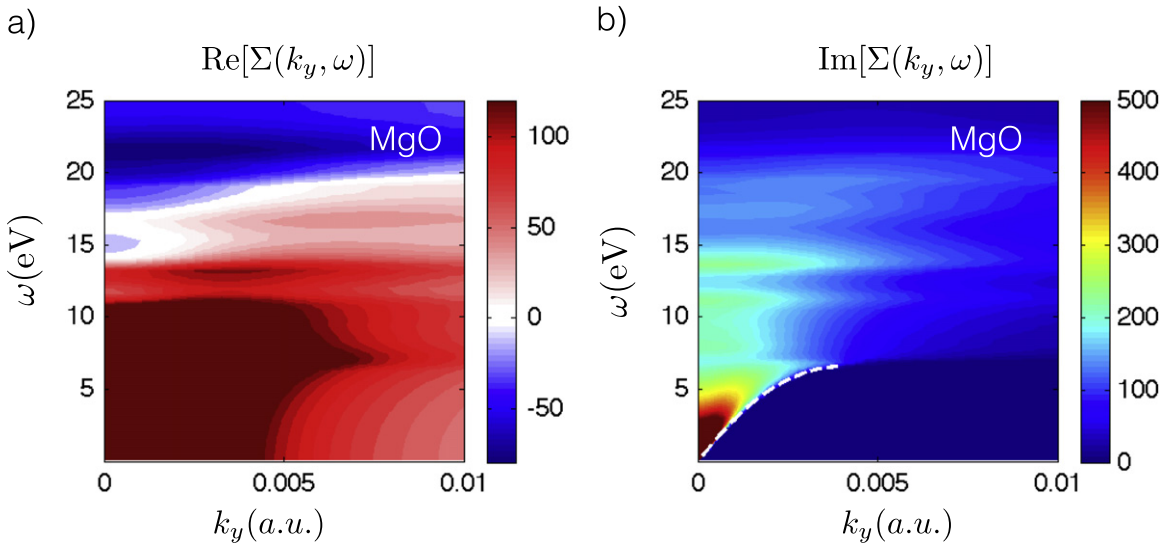

Figure 4. Color maps of (a) real and (b) imaginary parts of $\Sigma(k_y, \omega)$ function vs energy and parallel component of momentum k_y, for a 300 keV electron interacting with a MgO interface. Experimental values of the dielectric function have been used [25]. The k_y region where ν is purely imaginary is bounded by the dashed white line $k_y = \omega v^{-1}\sqrt{\epsilon(\omega)\beta^2 - 1}$.

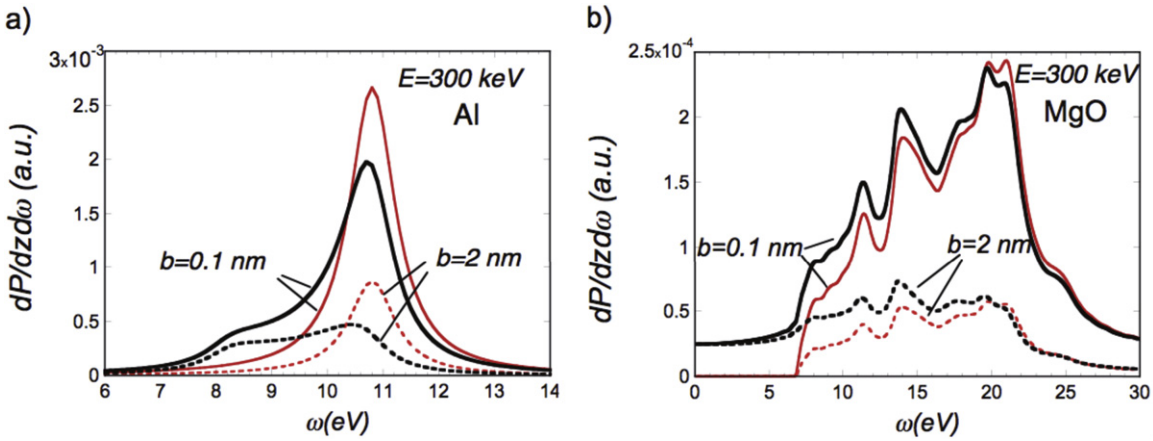

Figure 5. Retarded (black) and non-retarded (red) energy loss probability per unit length for a 300 keV electron probe moving parallel to (a) an Al interface described by a Drude function and (b) to a MgO interface. Continuous lines correspond to $b = 0.1$ nm, and dashed ones to $b = 2$ nm. Parameters of the Drude function are as in figure 2.

results are displayed for two values of the impact parameter. As mentioned above, for a given impact parameter, the region of the $k_y - \omega$ space significantly contributing to the interaction is loosely given by $\nu_0 b \lesssim 1$, a condition which limits the excitation spectrum into a window $\omega \lesssim \gamma v b^{-1}$ and $|k_y| \lesssim b^{-1}$. For the 300 keV electron probe under consideration, these limiting values are $k_y = 0.53$ a.u. and $\omega = 90$ eV for $b = 0.1$ nm, while for $b = 2$ nm those values are reduced down to $k_y = 0.03$ a.u. and $\omega = 4.5$ eV. In metallic targets, the consequences of retardation induced dispersion are clearly visualized in the EEL spectra of figure 5(a). In this

figure, while in the non-retarded approach (red lines) the spectra are centered at the surface plasmon energy (10.8 eV for Al), when retardation is considered (black lines), the spectrum is spread into a wider energy range. For the smaller impact parameter $b = 0.1$ nm, the intensity of the main peak is decreased, and a shoulder emerges around 8 eV, but for the higher impact parameter of 2 nm, the spectrum is clearly broadened and blue shifted.

In figure 5(b) we show the retardation effects in the EEL spectrum corresponding to MgO. Comparison with the non-retarded spectra reveals that the main consequence derived from the relativistic expressions is the presence of non-negligible losses in the energy region of the gap, which are due to the emission of CR. A striking feature of those plots is the weak impact parameter dependence of the radiative losses (compare continuous and dashed black lines). The components of the probe on the surface decay as the modified Bessel functions $K_0(\lambda b)$ and $K_1(\lambda b)$, where $\lambda = \omega/(\gamma v)$ (see for example [26]). For the present probe energy (300 keV), the decay length of the fields in the gap, λ^{-1}, is larger than 50 nm. Therefore, at small impact parameters the intensity of the exciting fields at the interface are rather similar, independently of the value of b. At large impact parameters, the softer decay of the low frequency fields means that radiation is the main inelastic channel contributing to the loss spectrum. The relevance of radiative losses at high impact parameters has been experimentally found in porous alumina [27, 28].

3. The character of the transversal component of the force

Let us focus now on the transversal component of the force acting on the probe electron, which is obtained from equation (1), involving the real part of the Σ function. First we study metallic targets, and then we consider insulators.

3.1. Transverse force in metallic interfaces

In figure 6 we represent, for two different probe energies, the impact parameter dependence of the transverse component of the force for a swift electron passing by an Al interface. We have plotted both electric and magnetic contributions to the Lorentz force as well as the non-retarded result. A remarkable result is that, although the total retarded force remains always attractive (negative), the electric contribution takes positive values near the surface ($b < 2$ nm for 300 keV electrons), being balanced by the attractive magnetic contribution, which turns out to be the leading term. The relevance of the magnetic force is still a more unexpected result in the 100 keV ($\beta = 0.55$) plot. Furthermore, the comparison of the total force plots shows that the retarded force is always weaker than the non-retarded one, except for a small range of b near the surface, where the retarded force is divergent. The divergent behavior of this force is a consequence of the local character of the dielectric function used in the current approach and might be corrected by imposing a cutoff in the momentum integral. It contrasts with the finite limit found by Muscat and Newns [11] for an electron gas, $F_x = -\omega_s^2/v^2$ as $b \to 0$. On the other hand, at large impact parameters one can numerically show that, in the limit $b \to \infty$, the transverse force $F_x(b) \to (4b^4\gamma)^{-1}$, a result which can be interpreted as the quasi-static limit of the image force. Based on the non-retarded expression (4), we analyze the role played by the surface plasmon in the transverse component of the force. First we notice that, for Drude metals, the surface response function $[\epsilon(\omega) - 1]/(\epsilon(\omega) + 1]$ takes positive or negative values (attractive or repulsive contributions to the force) depending on whether ω is smaller or larger

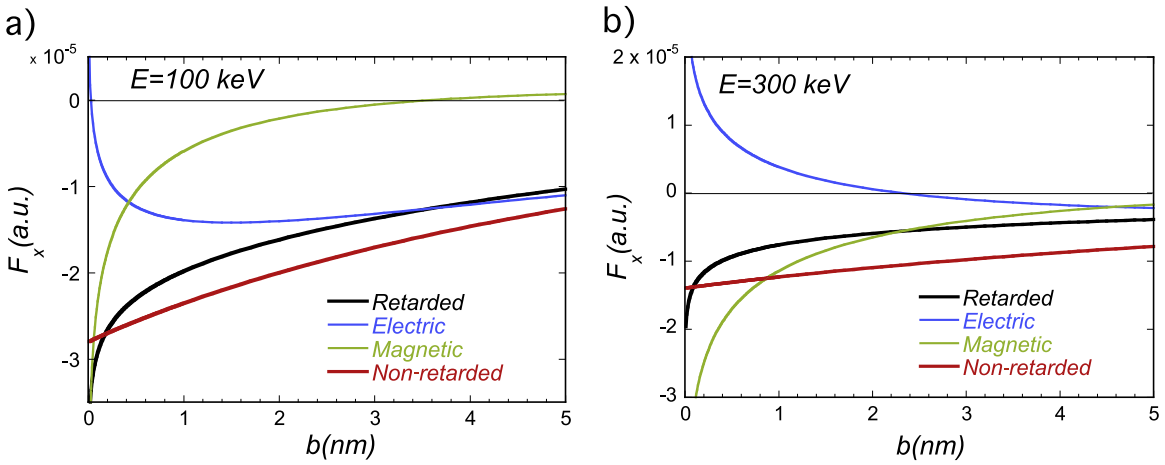

Figure 6. Transverse component of the force experienced by (a) a 100 keV and (b) a 300 keV electron moving parallel to an Al interface described by a Drude function (black line). The electric (blue line) and magnetic (green line) contributions to the Lorentz force have been also plotted. The red lines correspond to the non-retarded expression.

than ω_s. For frequencies below ω_s, the electron gas can follow the exciting field so that the corresponding induced surface charge density is in phase; therefore the contribution to the force is attractive. At frequencies above ω_s, the induced density is out of phase, and consequently the contribution is repulsive. The most striking difference between both retarded and non-retarded approaches is the divergent behavior of the retarded one at grazing incidence. Actually, the finite non-retarded limit is quite counter-intuitive if one thinks in terms of the image force acting on the probe. In the limit $b \to 0$ one can replace the Bessel function in equation (4) by the leading term of its series expansion, $K_1(x) \sim x^{-1}$, so that this equation reduces to:

$$F_x(b) = \frac{-1}{\pi v b} \int_0^\infty d\omega \, \mathrm{Re}\left[\frac{\epsilon(\omega) - 1}{\epsilon(\omega) + 1}\right]. \tag{10}$$

Then, by applying the K–K relation for the surface response function [29],

$$\mathrm{Re}\left[\frac{\epsilon(\omega) - 1}{\epsilon(\omega) + 1}\right] = -\frac{4}{\pi} \mathrm{P} \int_0^\infty \mathrm{Im}\left[\frac{-1}{\epsilon(\omega') + 1}\right] \frac{\omega'}{\omega^2 - \omega'^2} \mathrm{d}\omega', \tag{11}$$

where the symbol P stands for the Cauchy principal value. It is straightforward to prove that the integral of equation (10) vanishes for any causal dielectric function, so that in general the $b \to 0$ limit calculated in this way is not well defined. In the particular case of a Drude dielectric function, the integral of equation (4) can be calculated analytically [5]. Furthermore, the Bessel function in equation (4) works as an effective cutoff in the range of high ω values (repulsive contributions) in the integral, so that the non-retarded force is always attractive.

This argument points to the causality as the physical reason for the non-divergent limit of the transverse component of the non-retarded force and provides an intuitive explanation for its finite limit: in the local approach, causality implies that the induced charge density, the so-called *surface wake* [30], is located at the interface, just behind the probe, so that in the $b \to 0$ limit the resulting force is parallel to the velocity; i.e. it contributes basically to the stopping power. The induced charge density diverges as $b \to 0$, but the resulting force is balanced by the

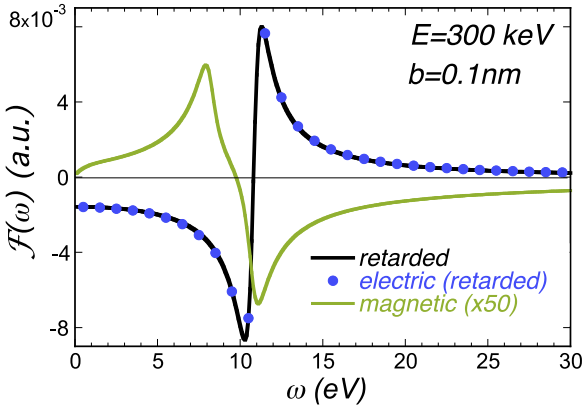

Figure 7. Spectral function $\mathcal{F}(\omega)$ of the transverse force experienced by a 300 keV electron moving parallel to an Al interface at impact parameters $b = 0.1$ nm. The black line corresponds to the total function, and the blue dots and green line represent its electric and magnetic contributions respectively. A factor 50 has been used in the magnetic contribution for the sake of clarity.

vanishing projection of the total force in the direction normal to the surface so that the product of both terms in equation (10) remains finite. In order to check the robustness of Muscat's limit [11], we have calculated the non-local corrections arising from the k dependence of the dielectric function in the specular reflection model [31, 32], and we have concluded that they are negligible in the range of probe energies of interest in electron microscopy. Actually, using the hydrodynamic dielectric function [33], we have found that the non-local correction to Muscat's value at the interface is about 3% for a 100 keV electron. Furthermore, the non-local corrections are still smaller as the velocity of the probe increases, so that one can safely consider that the Muscat's limit is physically sound. In the retarded theory, the balance between attractive and repulsive contributions to the total force is arguably broken so that it becomes divergent as $b \to 0$.

The physically relevant magnitude is the total Lorentz force. Nevertheless, it is helpful to analyze independently the splitting of this force into electric and magnetic terms. For this purpose we perform a spectral analysis of equation (1) by introducing the spectral function $\mathcal{F}(\omega)$, which represents the ω contribution to the force: $F_x = \int_0^\infty d\omega \mathcal{F}(\omega)$. In figure 7 we show this function (black line), together with its electric and magnetic contributions. Note that almost at any frequency the electric component is about two orders of magnitude larger than the magnetic one, so that the total force and the electric part are practically indistinguishable. Nevertheless, near the surface, the total magnetic force turns out to be the leading one, because the cancellation between attractive and repulsive contributions is much smaller than for the electric one. This fact can be visualized in table 1, which evidences the strong cancellation of contributions below and above ω_s, present in the integral of the electric part. Although in this table the differences between the retarded electric contribution and the non-retarded value are small, the balance between attractive and negative contributions reverses the sign of the total electric force.

The origin of the magnetic force is the current density induced in the medium. For probes close to the surface, the main contribution to the transverse force arises from the normal component of the current, which in its turn is proportional to the normal component of the

Table 1. Electric and magnetic contributions to the total Lorentz force below and above ω_s for a 300 keV electron traveling at a distance $b = 0.1$ nm from an Al interface (figure 7). The results corresponding to the retarded case have been added to allow comparison.

Contribution	$\int_0^{\omega_s} d\omega\mathcal{F}(\omega)$	$\int_{\omega_s}^{\infty} d\omega\mathcal{F}(\omega)$	$\int_0^{\infty} d\omega\mathcal{F}(\omega)$
Retarded electric	-0.117872×10^{-2}	0.119650×10^{-2}	0.1777×10^{-4}
Retarded magnetic	0.882746×10^{-5}	-0.401503×10^{-4}	-0.3132×10^{-4}
Non-retarded	-0.118676×10^{-2}	0.117297×10^{-2}	-0.1378×10^{-4}

electric field inside the medium. In the non-retarded limit, neglecting the damping, the field inside the target, just at the surface, is given by $E_x(x = 0_-, \omega) = \omega^2/(\omega^2 - \omega_s^2)E_x^{(p)}(x = 0, \omega)$, where $E_x^{(p)}(x = 0, \omega)$ stands for the electric field created by the probe at the surface. Furthermore, the leading contribution to these currents comes from the wake behind the probe. Notice that ω_s determines the crossover value for the direction of the induced current and thus for the magnetic force on the probe. Considering a positive probe, the currents are oriented toward the surface for $\omega < \omega_s$, and it is trivial to see that the corresponding magnetic force is attractive. For $\omega > \omega_s$, the force is reversed. Similar arguments explain the opposite sign of the electric and magnetic contributions to the force at the same energy.

In order to check the validity of the former results for other metals which are not properly described with a Drude dielectric function, we study the case of Au, a material which has been recently used in experiments showing the manipulation of metallic NPs by an electron beam [3]. Experimental data for different materials [34] covering a wide range of frequencies have been widely used in many theoretical approaches [4, 5]. Most of those dielectric data are obtained from optical or EELS measurements and, although in general they reproduce accurately EELS and light absorption spectra, in some cases they fail to reproduce the causal nature of the material response given by the K–K relations. Actually, we have checked that the tabulated values of Au provided in reference [34] do not fulfill the K–K relations, and we have considered the parameterization proposed by Werner *et al* [35]. These authors approximate the Au dielectric function by a set of nine Lorentzians:

$$\epsilon(\omega) = 1 + \sum_k \frac{A_k}{\omega_k^2 - \omega(\omega + i\Gamma_k)}, \tag{12}$$

where $k = 1,...,9$ and A_k, ω_k, and Γ_k are real parameters. The fact that this function has all the poles in the lower half ω-plane warrants its proper causal behavior. On the other hand, the bulk loss function calculated from this dielectric response is in reasonably good agreement with the one obtained from Palik's data [34].

In figure 8 we explore the dependence of the transverse force on the probe impact parameter. The plots of the electric and magnetic contributions, as well as the total retarded force, are qualitatively similar to the ones shown previously for the Drude function. The retarded plot also diverges as $b \to 0$, while it is numerically proven that in this limit the non-retarded force remains finite:

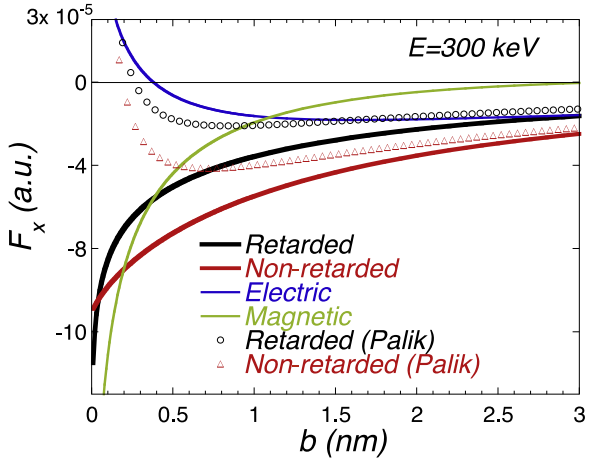

Figure 8. Transverse component of the force experienced by a 300 keV electron moving parallel to a Au interface described by the dielectric function of [35]. The electric (blue line) and magnetic (green line) contributions to the Lorentz force have also been plotted. Circles (∘) and triangles (Δ) correspond to the retarded and non-retarded plots calculated with the dielectric data by Palik [34].

$$\lim_{b\to 0} F_x = -\frac{1}{2v^2}\sum_k A_k, \tag{13}$$

so that near the surface the transverse force is related to the density of valence electrons of the target. Notice that the Muscat's limit may be considered as a particular case of equation (13).

To visualize the relevance of the causality of the response function, in figure 8 we have added the results of the calculation performed using Palik's data [34]. At large impact parameters, where most of the contribution to the force arises from the low ω region, both retarded and non-retarded plots are almost identical. This is a consequence of the relatively good agreement of both functions in the valence excitation region. Nevertheless, both the retarded and non-retarded plots turn out to be positive (repulsive force) at small values of b. In the non-retarded case, the origin of this positive value can be traced to the fact that the integral in equation (10) takes a non-vanishing negative value. This unphysical result also questions the reliability of the retarded plot obtained with Palik's data. The need for causally well-behaved dielectric functions has also been reported in the calculations of the Casimir forces between nanostructures [36, 37].

Palik's data have been used in the theoretical study of the crossover of the force exerted by STM electrons in small Au particles [20]. To check the effect of using a non-causal dielectric function for NPs, we have performed a preliminary calculation using the non-retarded expression for spheres [13], which demonstrates that both Palik's and Werner's dielectric functions lead to pretty similar plots of the transversal force in NPs of radius smaller than 5 nm. The differences for both responses increase for larger particles.

The same warning about the causality related behavior should be considered in calculations of the force performed with simplified response functions. For instance, in [16] authors study Cherenkov effects by using a constant (real) dielectric function, which obviously does not fullfil the K–K relations. Those results would be reliable only in the limit of very large impact parameters, where only the frequencies in the gap provide a significant contribution.

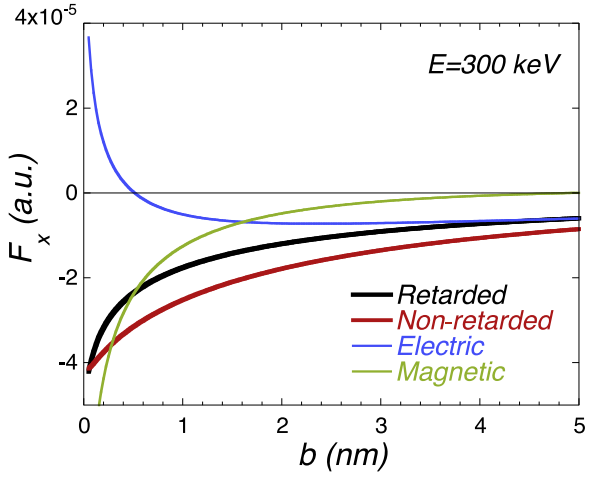

Figure 9. Transverse component of the force experienced by a 300 keV electron moving parallel to a MgO interface. The electric (blue line) and magnetic (green line) contributions to the Lorentz force have been plotted as well. The red line corresponds to the non-retarded expression.

Finally it is worth noting that, as pointed out above, Palik's data have been widely used to describe EELS and light scattering experiments of Au nanostructures [3, 20, 38, 39], but causality has little effect in those cases where the studied magnitude is a spectral function of ω, similarly to equation (7). Both Palik's and Werner's dielectric functions describe reasonably well the measured spectra. Moreover, when the longitudinal force is computed and integration over ω is required, contrary to the transverse force, it does not change its sign, because the contributions to the integral are positive in the whole ω-spectrum. Therefore, the resulting longitudinal force, although inaccurate, does not present the unphysical crossover in the sign shown in figure 8.

3.2. Transverse force in insulators

The case of insulators is of special interest, because they open the possibility of dynamic effects associated to the presence of radiation. In particular, we have chosen MgO because of the wideness of its gap and the large values of the real dielectric function there (the maximum is 7.3 at the gap edge). The experimental dielectric function considered [25] was derived from reflectance measurements and covers the energy spectrum up to 28 eV, a region where most of the valence electron excitations occur. The calculation procedure presented below ensures that the function safely verifies the K–K relations. We have extended the response above the highest tabulated data by means of a single Lorentzian function so that the resulting response is continuous and verifies the causality condition (vanishing of the integral in equation (10)). Because most of the structure of the dielectric function occurs in the tabulated region of ω, the precise extrapolation method has little influence on the fulfillment of the K–K relations.

In figure 9 we plot the transverse component of the force as a function of the impact parameter for a 300 keV electron traveling close to a MgO interface. The plots of the Lorenz force and its electric and magnetic components do not differ significantly from the case of metals studied in the previous section. Actually, the value of the force at grazing incidence is similar to that found for Al (figure 5), a result that supports the statement that the force near the

surface depends basically on the valence electron density of the target, as stated by equation (13). The fact that the force in insulators is similar to that of metals suggests that the crossover in the sign of the force found in metallic NPs, could also occur in dielectric nanotargets. The comparison with metallic targets at the same beam energy shows that for insulators, the magnetic component of the Lorentz force decreases faster with increasing impact parameters. This is a consequence of the reduction of the contributing ω range with increasing b, so that the response arises from the gap region, where the medium is an insulator.

4. The transverse force on extended beams

It is straightforward to generalize the current theory to the case of a spatially extended probe. We consider a beam represented by a stationary charge density $\rho(\mathbf{r})$, propagating with constant velocity $\mathbf{v}$ parallel to a flat interface. For the sake of simplicity we assume the charge density to be confined in the vacuum region and symmetric along the y and z axes, so that its Fourier transform $\rho(x, k_y, k_z)$ is real. Then the components of the total force experienced by the probe due to its interaction with the surface are written as follows:

$$F_x = \frac{-2}{\pi v}\int_0^\infty dx\int_0^\infty dx'\int_0^\infty dk_y\int_0^\infty d\omega\rho\left(x, k_y, \frac{\omega}{v}\right)\rho\left(x', k_y, \frac{\omega}{v}\right)\nu_0 \times \mathrm{Re}\left[\Sigma\left(k_y, \omega\right)\right]e^{-\nu_0(x+x')}, \tag{14}$$

$$F_z = \frac{-2}{\pi v}\int_0^\infty dx\int_0^\infty dx'\int_0^\infty dk_y\int_0^\infty d\omega\rho\left(x, k_y, \frac{\omega}{v}\right)\rho\left(x', k_y, \frac{\omega}{v}\right)\frac{\omega}{v} \times \mathrm{Im}\left[\Sigma\left(k_y, \omega\right)\right]e^{-\nu_0(x+x')}, \tag{15}$$

which obviously reduce to equations (1) and (2) for one point charge.

To visualize some consequences of the spatial extension, we consider a probe with a Gaussian distribution along the y axis at impact parameter b:

$$\rho(\mathbf{r}) = \frac{1}{\sqrt{2\pi}\sigma}\delta(x-b)\delta(z)e^{-\frac{y^2}{2\sigma^2}}. \tag{16}$$

Then, it is straightforward to write the total force as:

$$F_x = \frac{-2}{\pi v}\int_0^\infty d\omega\int_0^\infty dk_y e^{-\sigma^2k_y^2}\nu_0\,\mathrm{Re}\left[\Sigma\left(k_y, \omega\right)\right]e^{-2\nu_0 b}, \tag{17}$$

$$F_z = \frac{-2}{\pi v^2}\int_0^\infty \omega d\omega\int_0^\infty dk_y e^{-\sigma^2k_y^2}\,\mathrm{Im}\left[\Sigma\left(k_y, \omega\right)\right]e^{-2\nu_0 b}. \tag{18}$$

These expressions mean that the overall effect of the lateral extension of the probe derives from the reduction of the range of k_y contributing to the scattering. This reduction of the momentum space means that the effect of the beam extension is to be more relevant at small impact parameters, as suggested by the intuitive model of the image charge. For EELS in metallic targets, this cut-off not only represents a weakening of the interaction but also a stronger blue shift of the surface excitation spectrum due to the dispersion effect described in section 2.

Recently Rebernik [1] found that, whereas the force on a point charge is attractive toward the surface even at ultrarelativistic velocities, a charge packet may be repelled above a critical

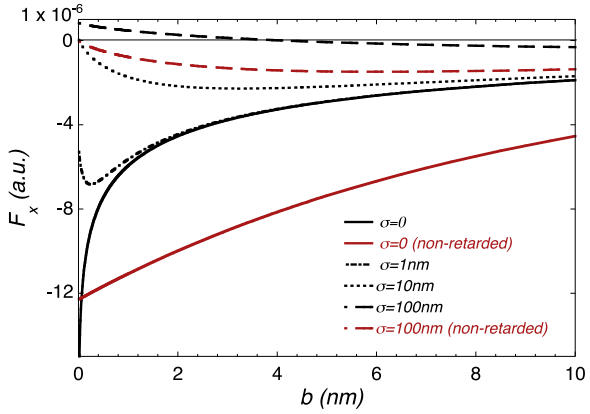

Figure 10. Transverse force experienced by a Gaussian electron probe of 400 keV extended sideways in the y direction and moving parallel to an Al interface, as a function of impact parameter b. Probes of different widths (different σ values) are considered and compared with the point electron beam $\sigma = 0$. The non-retarded expressions are also plotted for comparison in the extreme cases of $\sigma = 0$ and $\sigma = 100$ nm.

relativistic energy. In figure 10 we have checked this point by plotting the impact parameter dependence of the transverse component of the force for 400 keV beams of different widths corresponding to σ = 0, 1, 10, and 100 nm, moving in front of an Al surface. The force is attractive except for the widest beam of 100 nm. The non-retarded plots remain always attractive, showing that the reversal of the sign of the force is a relativistic effect. For such broad beams, the k_y space contributing to the force is reduced to an extremely narrow band near the origin, a region where the retardation induced dispersion is most noticeable (see figure 2). Given that the surface plasmon marks the border between attractive (below ω_s) and repulsive (above ω_s) forces, the balance of both contributions eventually turn out to be repulsive. Nevertheless, these broad beam configurations do not correspond with the beam conditions actually used in electron microscopy.

Furthermore, this approach, in which one does not account for the direct interaction among different elements of the beam packet, only makes sense in the case of a single particle; therefore its applicability is reduced to the quantum description of a single particle where the extension of the beam is given by the wave function of the probe $\Phi(\mathbf{r})$. Neglecting the momentum associated to the probe recoil, in the non-retarded approach it has been proven that the effects of the transverse extension of the beam in EELS quantum expressions can be reproduced by the classical theory by assuming that the probe transverse charge density is just the quantum probability [40]. The current approach may be considered an extension of the former theory to include the retardation effects in the response of the target.

5. The force on the surface and momentum conservation

In the actual STEM setup, only the longitudinal component of the force is probed, as far as the transverse one leads to deflection angles of the beam too small to be detected. The Muscat's limit provides a simple estimation of the angle deflection θ per unit length in metals at grazing incidence:

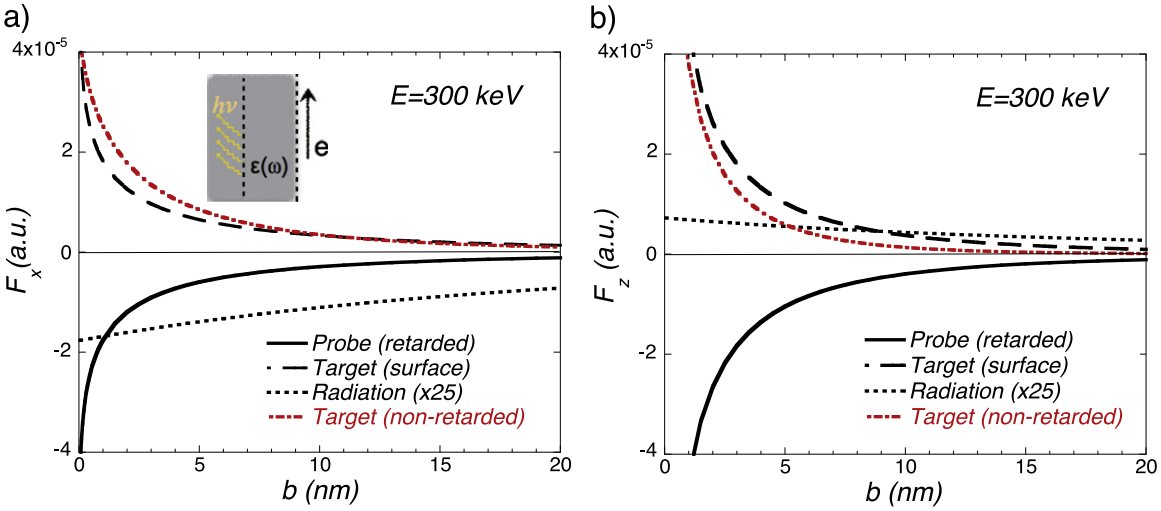

Figure 11. (a) Transverse and (b) longitudinal components of the force acting on a 300 keV probe (continuous black) and on a MgO target (black dashed). The black dotted line is the force associated to radiation (multiplied by a factor 25). For comparison the non-retarded forces on the target are plotted in the red dash-dotted line. In a) the inset sketches the surface used in the calculation of the force on the target.

$$\frac{\Delta\theta}{\Delta z} = \frac{\omega_s^2}{v^4}, \tag{19}$$

which for a typical STEM configuration, and assuming a 100 nm long target, leads to angles smaller than 10^{-5} rad, a value two orders of magnitude smaller than the typical acceptance semi-angle. Nevertheless, the effects of the interaction on small particles can be detected just as small displacements from their initial positions [3].

Contrary to the non-retarded theory, where momentum conservation implies that forces on both probe and target are equal, the relativistic theory adds radiation as a possible carrier of momentum and energy so that the strength of forces acting on the target and on the probe are not necessarily balanced.

The total force experienced by the target may be written in terms of the flux of the Maxwell stress tensor, T_{ij}, through its surface [26]. To calculate it, we consider the surface sketched in the inset of figure 11(a): it is a box with faces at $y, z = \pm\infty$, and lateral faces at the external side of the surface, $x = 0_+$, and at $x = -d$, where d is a distance large enough to ensure that all the evanescent components of the fields vanish. After some algebra, the components of the force are recast as double integrals in k_y and ω:

$$F_i = \frac{1}{4\pi^4 v}\int_0^\infty dk_y \int_0^\infty d\omega\ \mathrm{Re}\left[T_{ix}\left(x = 0_+,\, k_y,\, k_z = \frac{\omega}{v},\, \omega\right)\right.$$
$$\left. - T_{ix}\left(x = -d,\, k_y,\, k_z = \frac{\omega}{v},\, \omega\right)\right], \tag{20}$$

where the index i refers to x or z for the transverse or longitudinal components of the force, respectively. The components of the tensor are:

$$T_{ij}\left(x,\, k_y,\, k_z,\, \omega\right) = \begin{cases} \dfrac{1}{4\pi}\left\{\epsilon\left(\omega\right)E_i E_j^* + B_i B_j^* - \dfrac{1}{2}\left[\epsilon\left(\omega\right)\mathbf{E}\mathbf{E}^* + \mathbf{B}\mathbf{B}^*\right]\delta_{ij}\right\}, & \text{for } x < 0 \\ \dfrac{1}{4\pi}\left\{E_i E_j^* + B_i B_j^* - \dfrac{1}{2}\left[\mathbf{E}\mathbf{E}^* + \mathbf{B}\mathbf{B}^*\right]\delta_{ij}\right\}, & \text{for } x > 0. \end{cases} \quad (21)$$

With absolute generality it can be proved that the first integrals (at $x = 0_+$) in equation (20) are fully equivalent (up to the sign) to equations (1) and (2). This fact confirms that the flux through the left surface (at $x = -d$) is the force associated to radiation. Therefore, in the case of lossy media, where the flux through the left interface vanishes, we recover the action-reaction law: all the momentum lost by the probe is converted into mechanical momentum of the medium in a region of thickness Re $(\nu)^{-1}$ around the surface.

In the case of insulators, where CR becomes possible, both forces on the probe and the target differ in the term associated to the momentum of radiation, i.e. the second integral in equation (20). In figure 11 we show the balance between the three terms in both the transverse and longitudinal components of the force for a 300 keV electron interacting with a MgO target. The radiation is emitted inside the medium and forward (with respect to the probe trajectory), and therefore it does not emerge from the target. It means that CR has no effect on the dynamics of the target. The radiative contributions to both transverse and longitudinal components are small (they are multiplied by a factor 25 in the plots), a consequence of the low momentum carried by the radiation in the Cherenkov ω window. The small value of ω in the Cherenkov range also explains the fact that away from the surface, the radiative contribution to both components of the force decays more slowly than the force on the probe. Its effects on the longitudinal component of the force experienced by the probe are noticeable, as shown in figure 5(b). In the case of the transverse component of the force, CR introduces just a slight negative correction, which does not modify the sign of the total transverse force. It means that the attractive transverse force experienced by the target is stronger than that of the probe, while in the longitudinal direction the accelerating force on the target is weaker than the stopping force experienced by the probe.

Extension of these results to finite targets is not simple. On the one hand, CR radiation has been proven to provide noticeable contributions to EELS in a laterally bounded medium [27], showing that the boundaries of the target limit the CR spectrum to wavelengths compatible with the condition of propagating modes, consequently reducing the momentum carried by the radiation in comparison to that of the semi-infinite medium. Our computation shows that CR effects are too weak as to significantly affect the dynamics of the system, so that its contribution in a bounded target is expected to be negligible.

On the other hand, in a finite target there is the possibility of radiative decay of surface excitations, a channel that in the case of planar interfaces is forbidden by the mismatch between the dispersion relations of light and surface plasmons. The momentum transfer carried by the radiation is present in the full retarded calculations for spheres worked out by García de Abajo [41] and Howie and Reyes-Coronado *et al* [20], but it would be worthwhile to investigate its role in the total dynamics of the system.

6. Summary and conclusions

In this work we have studied the retardation effects in the dynamics of an electron probe interacting with a semi-infinite medium, with energy in the range of interest in STEM experiments. The focus has been placed on the sign of the transverse force, finding that for point probes it is always attractive. In metals, the most relevant retardation effects arise from the dispersion relation of the surface plasmon induced by the relativistic theory, while in insulators the effects derived from the possibility of radiation in the medium prove to produce the most noticeable differences. In general, we find that retardation effects tend to decrease the intensity of the transverse force except just at the interface, where the retarded expression gets divergent. In the study of the transverse force at small impact parameters, we have proved that the magnetic contribution is the leading one. In this problem, we have also pointed out the relevance of the causality of the dielectric function, warning about the need of checking this point when using tabulated data. Furthermore, we have found no substantial difference between the strength of the force in insulators and metals, an observation which suggests that insulator NPs would be manipulated in the same way as metallic ones.

We have extended the formalism to analyze the effect of the lateral extension of the probe, concluding that the transverse force can turn out to be repulsive for very broad beams, even at moderately relativistic velocities of the probe.

Finally, we have analyzed the effect of the radiation in the dynamics of the system. In the case of lossy media, where radiation is not allowed, the forces experienced by the target and the probe balance one another exactly, but in insulators under conditions allowing Cherenkov radiation, the magnitude of the transverse force acting on the target is larger than that acting on the probe.

Acknowledgments

Authors thank A Howie, R Barrera, and A Reyes-Coronado for many stimulating discussions. This project was supported by the ETORTEK project NANOIKER from the Basque Government (BG), project FIS2010-19609-C02-01 from the Spanish Ministry of Science and Innovation, and grant IT-75613 from BG-UPV/EHU. Computational resources were provided by DIPC (UPV/EHU, MICINN, BG, ESF).

Appendix A. Components of the electromagnetic field

In this work we use the following Fourier transform convention:

$$f(\mathbf{k}, \omega) = \int_{-\infty}^{\infty} d\mathbf{r} \int_{-\infty}^{\infty} dt\; e^{-i(\mathbf{k}\cdot\mathbf{r}-\omega t)} f(\mathbf{r}, t). \tag{A.1}$$

In the right region ($x > 0$), the electric and magnetic fields are easily calculated with the standard methods used in classical electrodynamics [42]:

$$
\begin{aligned}
E_x\left(x,\, k_y,\, k_z,\, \omega\right) &= -\alpha + 4\pi^2 \frac{\nu^2 - \epsilon\nu_0^2 - \nu\nu_o(\epsilon - 1)}{(\nu + \nu_0)(\nu + \epsilon\nu_0)} \delta\left(\omega - k_z v\right) e^{-\nu_0(x+b)} \\
E_y\left(x,\, k_y,\, k_z,\, \omega\right) &= -i\alpha \frac{k_y}{\nu_0} + i4\pi^2 k_y \frac{\nu_0\left(2\nu_0 + \nu\right)(\epsilon - 1) + \nu^2 - \epsilon\nu_0}{\nu(\nu + \nu_0)(\nu + \epsilon\nu_0)} \delta\left(\omega - k_z v\right) e^{-\nu_0(x+b)} \\
E_z\left(x,\, k_y,\, k_z,\, \omega\right) &= -i\alpha \frac{k_z}{\nu_0}\left(1 - \beta^2\right) + i4\pi^2 \frac{k_z}{(\nu + \nu_0)\nu_0} \left[\frac{2\nu_0^2(\epsilon - 1)}{\nu + \nu_0\epsilon} \right. \\
&\quad \left. + (\nu - \nu_0)\left(1 - \beta^2\right) \right] \delta\left(\omega - k_z v\right) e^{-\nu_0(x+b)} \\
B_x\left(x,\, k_y,\, k_z,\, \omega\right) &= i\alpha \frac{\beta k_y}{\nu_0} - i4\pi^2 \frac{\beta k_y(\nu - \nu_0)}{\nu_0(\nu + \nu_0)} \delta\left(\omega - k_z v\right) e^{-\nu_0(x+b)} \\
B_y\left(x,\, k_y,\, k_z,\, \omega\right) &= -\alpha\beta - \frac{4\pi^2\beta}{\nu + \nu_0} \left[\frac{2k_z^2(\epsilon - 1)}{\nu + \epsilon\nu_0} + \nu - \nu_0 \right] \delta\left(\omega - k_z v\right) e^{-\nu_0(x+b)} \\
B_z\left(x,\, k_y,\, k_z,\, \omega\right) &= 8\pi^2 \frac{\beta k_y k_z(\epsilon - 1)\delta\left(\omega - k_z v\right)}{(\nu + \nu_0)(\nu + \epsilon\nu_0)} \delta\left(\omega - k_z v\right) e^{-\nu_0(x+b)},
\end{aligned}
\tag{A.2}
$$

where $\alpha = 4\pi^2\delta(\omega - k_z v)e^{-\nu_0|x-b|}$ and β, ν, and ν_0 are defined in section 2. In these equations we have split the fields into the direct (the terms containing the factor α) and induced fields. Inside the medium ($x < 0$), the components of the electromagnetic field are:

$$
\begin{aligned}
E_x\left(x,\, k_y,\, k_z,\, \omega\right) &= -8\pi^2 \frac{\nu_0}{\nu + \epsilon\nu_0} \delta\left(\omega - k_z v\right) e^{-\nu_0 b} e^{\nu x} \\
E_y\left(x,\, k_y,\, k_z,\, \omega\right) &= -i8\pi^2 \frac{k_y}{\nu + \epsilon\nu_0} \delta\left(\omega - k_z v\right) e^{-\nu_0 b} e^{\nu x} \\
E_z\left(x,\, k_y,\, k_z,\, \omega\right) &= -i8\pi^2 \frac{k_z\left[\nu\left(1 - \beta^2\right) + \nu_0\left(1 - \beta^2\epsilon\right)\right]}{(\nu + \nu_0)(\nu + \epsilon\nu_0)} \delta\left(\omega - k_z v\right) e^{-\nu_0 b} e^{\nu x} \\
B_x\left(x,\, k_y,\, k_z,\, \omega\right) &= i8\pi^2 \frac{\beta k_y \delta\left(\omega - k_z v\right)}{\nu + \nu_0} e^{-\nu_0 b} e^{\nu x} \\
B_y\left(x,\, k_y,\, k_z,\, \omega\right) &= -8\pi^2 \frac{\beta\delta\left(\omega - k_z v\right)}{(\nu + \nu_0)(\nu + \epsilon\nu_0)} \left[(\epsilon - 1)k_z^2 + \nu(\nu + \epsilon\nu_0) \right] e^{-\nu_0 b} e^{\nu x} \\
B_z\left(x,\, k_y,\, k_z,\, \omega\right) &= 8\pi^2 \frac{\beta k_y k_z(\epsilon - 1)\delta\left(\omega - k_z v\right)}{(\nu + \nu_0)(\nu + \epsilon\nu_0)} e^{-\nu_0 b} e^{\nu x}.
\end{aligned}
\tag{A.3}
$$

References

[1] Rebernik R P 2012 *Phys. Rev. Lett.* **109** 244801

[2] Rebernik R P and Podgornik R 2013 *EPL* **102** 24001

[3] Batson P E, Reyes-Coronado A, Barrera R G, Rivacoba A, Echenique P M and Aizpurua J 2012 *Ultramicroscopy* **123** 50

[4] García de Abajo F J 2010 *Rev. Mod. Phys.* **82** 209
[5] Rivacoba A, Zabala N and Aizpurua J 2000 *Prog. in Surf. Sci.* **65** 1–64
[6] Rodríguez-González B, Attouchi F, Fernanda C M, Myroshnychenko V, Stéphan O, García de Abajo F J, Liz-Marzán L M and Kociak M 2012 *Langmuir* **28** 9063
[7] Koh A L, Fernández-Domínguez A I, McComb D W, Maier S A and Yang J K W 2011 *Nano Lett.* **11** 1323
[8] Cowley J M 1982 *Ultramicroscopy* **9** 231
[9] Cowley J M 1986 *Prog. Surf. Sci.* **21** 209
[10] Howie A 1983 *Ultramicroscopy* **11** 141
[11] Muscat J P and Newns D M 1977 *Surface Sci.* **64** 461
[12] Echenique P M and Howie A 1985 *Ultramicroscopy* **16** 269
[13] Rivacoba A and Echenique P M 1988 *Ultramicroscopy* **26** 389
[14] García-Molina R, Gras-Marti A, Howie A and Ritchie R H 1985 *J. Phys.* C **18** 5335
[15] Forstmann F, Gras-Marti A, Ferrell T L, Warmack R J and Mandola K C 1991 *Phys. Rev.* B **44** 4884
[16] Schieber D and Schätcher L 1998 *Phys. Rev.* E **57** 6008
[17] García de Abajo F J 2004 *Phys. Rev.* B **70** 115422
[18] Batson P E, Reyes-Coronado A, Barrera R G, Rivacoba A, Echenique P M and Aizpurua J 2011 *Nano Lett.* **11** 3388
[19] Vesseur E J R, Aizpurua J, Coenen T, Reyes-Coronado A, Batson P E and Polman A 2012 *MRS Bulletin* **37** 752
[20] Reyes-Coronado A, Barrera R, Batson P E, Echenique P M, Rivacoba A and Aizpurua J 2010 *Phys. Rev.* B **82** 235429
[21] Ritchie R H 1981 *Philos. Mag.* A **44** 931
[22] Ritchie R H and Howie A 1988 *Philos. Mag.* A **58** 753
[23] Sonnentag P and Hasselbach F 2007 *Phys. Rev. Lett.* **98** 200402
[24] Howie A 2011 *Ultramicroscopy* **111** 761
[25] Roessler D M and Walker W C 1967 *Phys. Rev.* **159** 733
[26] Jackson J D 1998 *Classical Electrodynamics* (New York: Wiley)
[27] Zabala N, Pattantyus-Abraham A G, Rivacoba A, Garcia de Abajo F J and Wolf M O 2003 *Phys. Rev.* B **68** 245407
[28] García de Abajo F J, Pattantyus-Abraham A G, Zabala N, Rivacoba A, Wolf M O and Echenique P M 2003 *Phys. Rev. Lett.* **91** 143902
[29] Tan G L, de Noyer L K, French R H, Guittet M J and Gautier-Soyer M 2004 *J. of Electr. Spectr. and Rel. Phen.* **142** 77
[30] Garcia de Abajo F J and Echenique P M 1992 *Phys. Rev.* B **45** 8771
[31] Ritchie R H and Marusak A L 1966 *Surf. Sci.* **4** 234
[32] Zabala N and Echenique P M 1990 *Ultramicroscopy* **32** 327
[33] Pines D and Nozieres P 1966 *The Theory of the Quantum Liquids* (New York: Benjamin)
[34] Palik E D 1985 *Handbook of Optical Constants of Solids* (Orlando, FL: Academic Press)
[35] Werner W S M, Glantschnig K and Ambrosch-Draxi C 2009 *J. Phys. Chem. Ref. Data* **38** 1013
[36] Bimonte G 2011 *Phys. Rev.* A **83** 042109
[37] Shpak O and Palasantzas G 2011 *Phys. Rev.* A **84** 044501
[38] Neubrech F, García-Etxarri A, Weber D, Bochterle J, Shen H, Lamy de la Chapelle M, Bryant G W, Aizpurua J and Pucci A 2010 *Appl. Phys. Lett.* **96** 213111
[39] Lassiter J B, Aizpurua J, Hernandez L I, Brandl D W, Romero I, Lal S, Hafner J H, Nordlander P and Halas N J 2008 *Nano Lett.* **8** 1212
[40] Zabala N and Rivacoba A 1993 *Phys. Rev.* B **48** 14534
[41] García de Abajo F J and Howie A 1998 *Phys. Rev. Lett.* **80** 5180
[42] Stratton J S 1941 *Electromagnetic Theory* (New York: McGraw-Hill)